JOURNAL OF GEOPHYSICAL RESEARCH, VOL. 107, NO. A12, 1488, doi:10.1029/2001JA000306, 2002

Sources of the solar wind at solar activity maximum

M. Neugebauer,[1] P. C. Liewer, and E. J Smith
Jet Propulsion Laboratory, California Institute of Technology, Pasadena, California, USA

R. M. Skoug
Los Alamos National Laboratory, Los Alamos, New Mexico, USA

T. H. Zurbuchen
University of Michigan, Ann Arbor, Michigan, USA

Received 20 September 2001; revised 2 December 2001; accepted 7 December 2001; published 28 December 2002.

[1] The photospheric sources of solar wind observed by the Ulysses and ACE spacecraft from 1998 to early 2001 are determined through a two-step mapping process. Solar wind speed measured at the spacecraft is used in a ballistic model to determine a foot point on a source surface at a solar distance of 2.5 solar radii. A potential-field source-surface model is then used to trace the field and flow from the source surface to the photosphere. Comparison of the polarity of the measured interplanetary field with the polarity of the photospheric source region shows good agreement for spacecraft latitudes equatorward of 60°. At higher southern latitudes, the mapping predicts that Ulysses should have observed only outward directed magnetic fields, whereas both polarities were observed. A detailed analysis is performed on four of the solar rotations for which the mapped and observed polarities were in generally good agreement. For those rotations, the solar wind mapped to both coronal holes and active regions. These findings for a period of high solar activity differ from the findings of a similar study of the solar wind in 1994–1995 when solar activity was very low. At solar minimum the fastest wind mapped to the interior of large polar coronal holes while slower wind mapped to the boundaries of those holes or to smaller low-latitude coronal holes. For the data examined in the present study, neither spacecraft detected wind from the small polar coronal holes when they existed and the speed was never as high as that observed by Ulysses at solar minimum. The principal difference between the solar wind from coronal holes and from active regions is that the O^{7+}/O^{6+} ion ratio is lower for the coronal hole flow, but not as low as in the polar coronal hole flow at solar minimum. Furthermore, the active-region flows appear to be organized into several substreams unlike the more monolithic structure of flows from coronal holes. The boundaries between plasma flows from neighboring sources are marked by large magnetic holes, plasma sheets, and low entropy, independent of whether the sources have the same or opposite magnetic polarities. The evolution of solar wind properties between 1 AU and the 1.6–5.4 AU solar distance of Ulysses is also briefly discussed. *INDEX TERMS:* 2169 Interplanetary Physics: Sources of the solar wind; 2164 Interplanetary Physics: Solar wind plasma; 2162 Interplanetary Physics: Solar cycle variations (7536); *KEYWORDS:* solar wind sources, solar active regions, coronal holes

Citation: Neugebauer, M., P. C. Liewer, E. J. Smith, R. M. Skoug, and T. H. Zurbuchen, Sources of the solar wind at solar activity maximum, *J. Geophys. Res.*, *107*(A12), 1488, doi:10.1029/2001JA000306, 2002.

1. Introduction

[2] Between November 1994 and September 1995, the Ulysses spacecraft moved from a solar latitude of 80°S across the equator to 80°N. It was a period of low solar activity. *Neugebauer et al.* [1998] used several methods to map the solar wind observed by the Ulysses and Wind spacecraft to the solar surface to study how the properties of the solar wind depended on where it came from. Their results indicated that the fastest solar wind emanated from deep within the north and south polar coronal holes. Slower wind mapped to either the outer boundaries of the polar coronal holes or to smaller coronal holes at low solar latitudes.

[3] In this paper we apply some of the same methods as those used by *Neugebauer et al.* [1998] to study the sources

[1]Now at Lunar and Planetary Laboratory, University of Arizona, Tucson, Arizona, USA.

0148-0227/02/2001JA000306

of the solar wind during a period of rising and high solar activity. The goal is to determine the dependence of solar wind structures and sources on the level of solar activity. The task is more difficult at solar maximum because of the greater complexity and greater temporal variability of the solar magnetic field, including transient events which interrupt the quasistationary flows we wish to study. Both Ulysses and ACE data are used in the analysis to provide insight into the dependence on solar latitude. The period covered is 1998 through early 2001.

[4] Section 2 is a description of the mapping procedure and compares the polarity of the heliospheric magnetic field (HMF) predicted by the mapping to the HMF polarity observed by Ulysses over the solar latitude range 6°S to 80°S. The photospheric sources of the solar wind observed by Ulysses and ACE over four solar rotations are presented and discussed in section 3. Some of the wind maps to coronal holes while some of it maps to active regions. The similarities and differences between the solar wind from coronal holes and the solar wind from active regions are presented in section 4. Although maps and parameter plots are presented for only one of the four rotations analyzed, all four rotations were used in the analysis. Section 5 is a consideration of the boundaries between solar wind streams from different sources, and section 6 is a consideration of the evolution of the solar wind streams as they move from 1 AU to Ulysses. Finally, the principal results are summarized and discussed in section 7.

2. Two-Stage Mapping Procedure

[5] Except where otherwise noted, the analyses in this paper are based on 1-hour averages of solar wind plasma and magnetic field parameters measured by the Ulysses spacecraft in a near polar heliocentric orbit and the ACE spacecraft on a halo trajectory about the Sun-Earth L1 Lagrangian point. The solar wind speed measured at each spacecraft is used to map the wind back to 2.5 solar radii (R_s) on the assumption of radial flow at constant speed. While such a ballistic model may seem oversimplified, it works remarkably well because the effect of the solar wind coming up to speed is roughly equal and opposite to the effect of the initial corotation, leading to an estimated overall accuracy of ~10° in longitude [*Nolte and Roelof*, 1973]. Inward magnetohydrodynamic (MHD) mapping from a spacecraft toward the Sun by *Pizzo* [1981] and by *Riley et al.* [1999] show that the ballistic model is inadequate for describing the temporal or spatial profiles of plasma parameters on the leading edge of high-speed streams, and they find ~20° differences between the MHD and the ballistic solutions for the longitudes of the stream fronts. We note, however, that while these MHD models take account of the continuing acceleration of the solar wind as it flows out from the Sun, they do not include the effect of initial corotation. MHD models that do include corotation effects are currently under development. In the meantime, if one is interested only in source longitudes, but not in stream profiles, the ballistic model may perhaps provide as good an approximation as do the MHD models used to date.

[6] In the next step we use a potential-field source-surface (PFSS) model to trace the magnetic field (and, by assumption, the plasma streamlines) from the source surface at 2.5 R_s to the photosphere. In such a model [*Schatten et al.*, 1969; *Hoeksema*, 1989] the field is calculated between an inner boundary at the photosphere where the line-of-sight field is determined by magnetograph observations and an outer boundary at the source surface. The field is forced to be radially directed at the outer boundary. Except where noted otherwise, the inner boundary conditions are based on the Kitt Peak National Observatory (KPNO) synoptic magnetograms (available at ftp://argo.tuc.noao.edu/kpvt/synoptic/mag/) at nearly their full resolution of 1° × 1° over the complete latitude-longitude range of 180° × 360°. We then use a potential field solver developed by Z. Mikic which employs finite differences in radius and latitude and Fourier transforms in longitude. We set the resolution to (nr, nlat, nlong) = (101, 151, 256) corresponding to about 75 modes in latitude and 128 modes in longitude. As proposed by *Wang and Sheeley* [1992], the radial component of the calculated field at the inner boundary is matched to the radial component of the measured photospheric field.

[7] The synoptic magnetographs slowly change from one solar rotation to the next. We have assigned the mapped-back spacecraft data to the Carrington rotation corresponding to the calculated time t_{sun} when the plasma left the Sun, where $t_{sun} = t_{sc} - R/V$, t_{sc} is the time of observation at the spacecraft, R is solar distance and V is the measured solar wind speed. Because, unlike the Earth and ACE which circle the Sun, Ulysses' orbit is approximately fixed in inertial space, there is a small interval of overlap or longitudinal duplication of Ulysses data in each Carrington rotation. (An alternative option would be to use "leap rotations" as discussed by *Posner et al.* [2001]).

[8] There are several ways to check the reliability of the mapping. One is to compare the latitude and longitude of open field lines calculated by the mapping procedure to the latitude and longitude of coronal holes observed in the He 1083 nm line. We show evidence of such agreement in a following figure. Another test of the mapping is to compare the magnetic polarity of the calculated solar wind source to the polarity of the magnetic field observed at ACE or Ulysses. Figure 1 provides such a comparison for Ulysses as joint functions of time and solar latitude and longitude. On the left side of the figure is a plot of the latitude of Ulysses as a function of time (in units of Carrington rotations) from January 1998 through July 2001. The middle panel shows the polarity of the heliospheric magnetic field observed by Ulysses mapped back to the source surface at 2.5 R_s. The following steps were used to generate this panel. The radial and tangential components of the HMF, B_R and B_T, were averaged over 12-hour intervals. The magnetic polarity P is the cosine of the angle between the average field direction in the RT plane and the expected direction of an outward directed Parker spiral. Specifically,

$$P = (B_R - \Omega R \cos\lambda B_T/V)/\left[\sqrt{\left(1 + (\Omega R \cos\lambda/V)^2\right)}\sqrt{\left(B_R^2 + B_T^2\right)}\right], \quad (1)$$

where Ω is the solar rotation rate and λ is heliographic latitude. We chose to use a latitude-independent value of $\Omega = 2.7 \times 10^{-6}$ s^{-1} (corresponding to a sidereal rotation period of 25.4 days) for two reasons: (1) The 10% difference in the

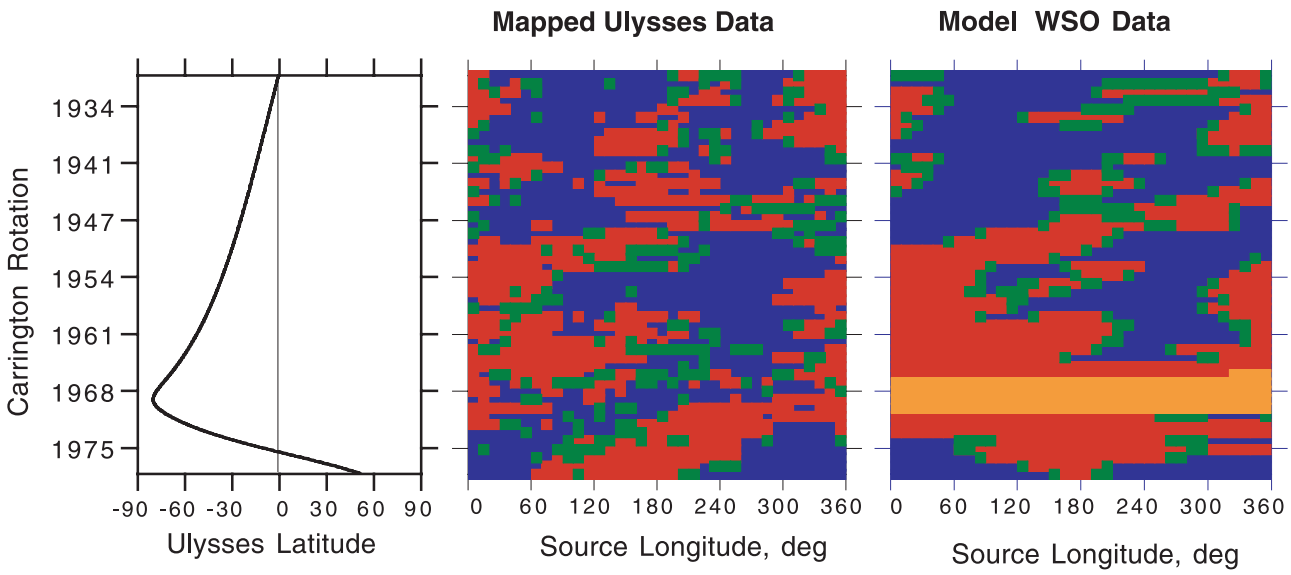

Figure 1. (left) Variation of the latitude of the Ulysses spacecraft as a function of Carrington rotation number. (middle) The magnetic polarity of the heliospheric magnetic field observed by Ulysses as a function of the mapped-back Carrington rotation number and longitude on a source surface at 2.5 solar radii. (right) The magnetic polarity expected at the Ulysses foot point on the source surface on the basis of the potential-field source-surface model provided by the Wilcox Solar Observatory. Red denotes outward fields, blue denotes inward fields, green denotes mixed magnetic polarity, and orange denotes implied outward fields.

rate of rotation of the solar magnetic field between 0 and 45° latitude [*Snodgrass*, 1983] changes P by ≤ 0.02 for $R \leq 5.4$ AU and $V \geq 300$ km/s, and (2) the boundaries of coronal holes usually don't exhibit latitudinal differential rotation. The wind is mapped back to the source surface assuming radial flow at speed V and then the 12-hour values of P are binned in 10° intervals of Carrington longitude on the source surface. An outward (inward) polarity with $P > 0$ ($P < 0$) is plotted in red (blue) if all the mapped-back values of P in a bin have the same polarity. If there are two or more 12-hour values of P in a bin that do not all have the same polarity, the polarity is said to be mixed and is plotted in green. If a bin has no 12-hour value of P, it is assigned the polarity of the time-wise-preceding (greater longitude) bin. Almost a quarter of the polarity changes shown in the center of Figure 1 occurred across such a gap, but for 84% of those changes, the filled-in gap was only 10° or 20° wide.

[9] The right-hand panel of Figure 1 shows the polarity of the HMF predicted to be observed by Ulysses on the basis of the Wilcox Solar Observatory (WSO) source-surface field. In this model, the source surface is located at 2.5 R_s and is based on the assumption that the photospheric field is in the radial direction. We used this data source because plots of the location of the heliospheric current sheet (HCS) are readily available over the internet (at http://quake.stanford.edu/~wso/coronal.html) and the 5° resolution is adequate for the purpose of this figure. The source-surface foot points of the Ulysses trajectory were overlaid on the source-surface field maps to determine the direction of the expected field. As in the Ulysses data plot, outward fields are denoted by red and inward fields by blue. The polarity is plotted as mixed (green) for fields within one contour level (±1 μT) of the neutral sheet. The latitudinal range of the WSO maps is only ±70°; the orange band in the right-hand panel corresponds to CR 1967–1971 when Ulysses was poleward of −70° and the source-surface maps show only outward fields at its −70° boundary. We generated source-surface field maps from the higher-resolution KPNO magnetograms for CR 1967–1971 and found that they also indicate that the HCS was equatorward of −70° for those rotations.

[10] Although the two polarity diagrams in Figure 1 differ in detail, the overall patterns are quite similar through CR 1964. For CR 1965–1973, when Ulysses was poleward of −60°, the model predicts almost purely outward fields, whereas Ulysses continued to observe a mix of magnetic polarities. In what follows, we concentrate on a limited number of those rotations for which Ulysses was equatorward of −60° and the observed and modeled polarities were in general agreement.

[11] *Neugebauer et al.* [1998] studied the location of the HCS using an MHD model and many different PFSS models based on different source surface radii, different photospheric boundary conditions, different sources of magnetograph data, and with/without a current sheet external to the source surface. The envelope of all the current sheets calculated by all those different methods had a latitudinal spread of up to 22°and about a 10° spread in the longitudes of their latitudinal extrema. Many of those PFSS models are no longer used because of poor fits to the near-Earth data. For the purpose of the present paper it is relevant to note from Figure 3f of *Neugebauer et al.* [1998] that the "SS-W&S" model, which has the same boundary conditions as in the present work, locates the latitude of the

Table 1. Location of Ulysses During Carrington Rotations Included in This Study

Carrington Rotation	Date at Sun, day/year	Solar Distance, AU	Latitude, degree	Longitude,[a] degree
1934	77/1998–104/1998	5.4	−6	335
1946	39/1999–66/1999	5.1	−23	324
1953	230/1999–257/1999	4.6	−34	196
1957	339/1999–1/2000	4.1	−42	83

[a] The source-surface longitude of the Ulysses foot point at the start of the Carrington rotation when the ACE foot point is at 360°.

HCS within 4° of the latitude calculated from the MHD model.

3. Solar Wind Sources

[12] We have carried out detailed analyses for four solar rotations picked on the basis of good overall agreement between the magnetic polarity of the HMF observed by Ulysses together with agreement between optical coronal holes and open field regions as determined by the PFSS model. Table 1 presents the dates of the solar observations, the solar distance and latitude of Ulysses, and the longitudinal separation of Ulysses and ACE for the four rotations. We use CR 1953 to illustrate our analysis methods.

[13] Figure 2a shows solar data for CR 1953. The red and blue background splotches indicate the field strength from the KPNO high-resolution synoptic magnetograph for that rotation. As in Figure 1, red (blue) denotes outward (inward) fields. Active regions appear as concentrations of strong fields, paired into leading and following polarities appropriate to the solar hemisphere. The boundaries of coronal holes determined from observations in the wavelength of He 1083 nm and their magnetic polarities are indicated on the figure in black; these data are also supplied by KPNO and are available online at ftp://argo.tuc.noao.edu/kpvt/synoptic/choles/. For the purpose of the ensuing discussion, we call a region a coronal hole if it has been so identified from the He 1083 nm observations, and we call a region an active region if it is a region of strong fields. Note in Figure 2a that there is essentially no overlap between the two features, although active regions are commonly found near coronal holes. PFSS models often indicate the presence of open field lines emerging from active regions, but we do not call such regions coronal holes.

[14] The contours in Figure 2b indicate the photospheric magnetic field in Figure 2a mapped to the source surface on the basis of the PFSS model. Contours of outward field strength are shown as solid red curves, while the dotted blue curves represent inward fields. The HCS is shown as a dashed green line; note how close the current sheet comes to the poles, in contrast to the nearly equatorial location of the current sheet near solar minimum. The crosses in Figure 2b denote the source-surface foot points of ACE (near the equator) and Ulysses (at 33.2°S to 35.4°S). One foot point has been drawn for each 3° of longitude on the source surface; note the overlapping Ulysses data near 190° which results from our method of assigning Carrington rotation numbers to the Ulysses data. The magnetic polarities of the fields measured at the spacecraft are also coded in red and blue for outward and inward magnetic polarities, respectively. Hourly averaged data were used to determine polarity, and the gaps in the Ulysses foot points result from empty 3° bins caused by steeply rising speeds. Agreement between the measured and the modeled polarities is generally very good except that the observed polarity reversals are sometimes somewhat displaced from the model current sheet. Such a displacement is not surprising because the source-surface fields near the current sheet are usually very weak and the location of the sheet can vary from one PFSS model to another. Figure 2b also shows occasional hours of unexpected polarities well inside a magnetic sector, perhaps caused by large-amplitude Alfvén waves or major kinks in the field.

[15] Figure 2c superimposes the results of the two-stage mapping of ACE and Ulysses data to their photospheric sources on the solar data repeated from Figure 2a. The arrows indicate the sources of the solar wind observed by ACE (upper set of arrows) and Ulysses (lower set). The tail of each arrow is the spacecraft foot point on the source surface as determined by the ballistic mapping, while the arrow's head shows the region on the Sun from which the open field lines threading the spacecraft originate as determined by the PFSS mapping. In a few instances (e.g., for Ulysses at 110°–120° longitude), the polarity (color) of the arrow does not match the polarity of the source region, which means that the mapping must be wrong. But most of the time the colors of the arrows and the magnetograph data agree. Some of the solar wind maps to coronal holes (CH); examples for CR 1953 are ACE at longitudes of 80°–120° and Ulysses at longitudes >280°. In other instances, the

Figure 2. (opposite) (a) Magnetogram and coronal hole data for CR 1953. The background red and blue features show the photospheric magnetic field strength as measured by KPNO. The black lines show the boundaries of coronal holes as determined by observations in He 1083 nm. The field polarity is indicated by red (outward fields) or blue (inward) in the magnetograph data and by plus (outward) or minus (inward) signs for the coronal holes. (b) The foot points of the solar wind observed by ACE and Ulysses mapped to a source surface at 2.5 R_s, with the magnetic polarity denoted by red (outward), blue (inward), or green (near the current sheet) crosses. In the background is the source-surface magnetic field calculated from KPNO magnetograph data; outward fields are shown as solid red lines, inward fields as dotted blue lines, and the heliospheric current sheet as a dashed green line. The numbers on the contours indicate the strength of the magnetic field on the source surface as calculated by the potential field model. (c) The same as Figure 2a with the superposition of arrows whose feet denote the source-surface foot points of the solar wind observed by ACE (upper set of arrows) and Ulysses (lower arrows). The arrow heads indicate the photospheric location of the field line threading each of the foot points. The arrows are colored according to the observed polarity of the HMF: red for outward, blue for inward, and green for mixed polarity.

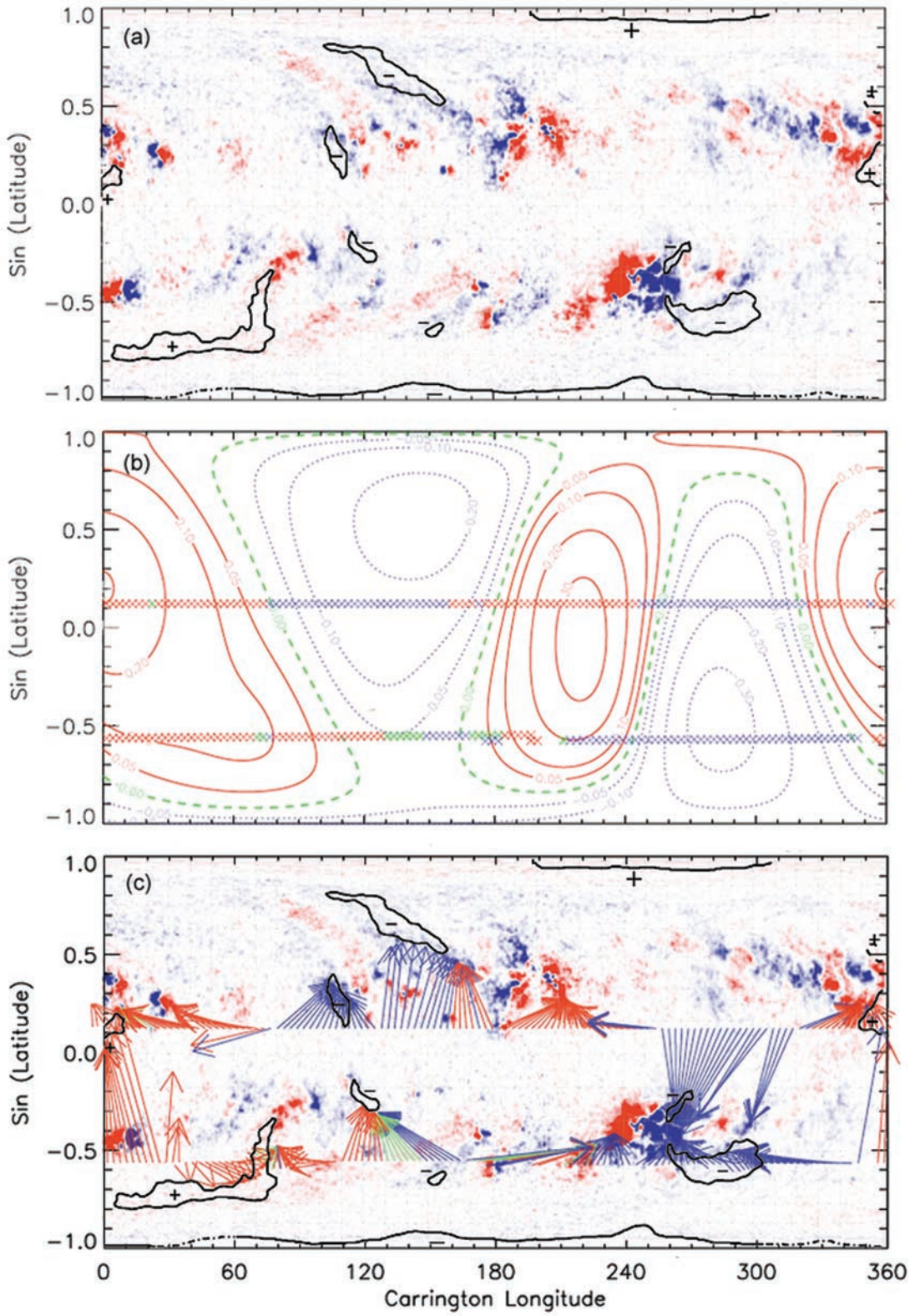
(a)
(b)
(c)
Sin (Latitude)
1.0
0.5
0.0
−0.5
−1.0
0
60
120
180
240
300
360
Carrington Longitude

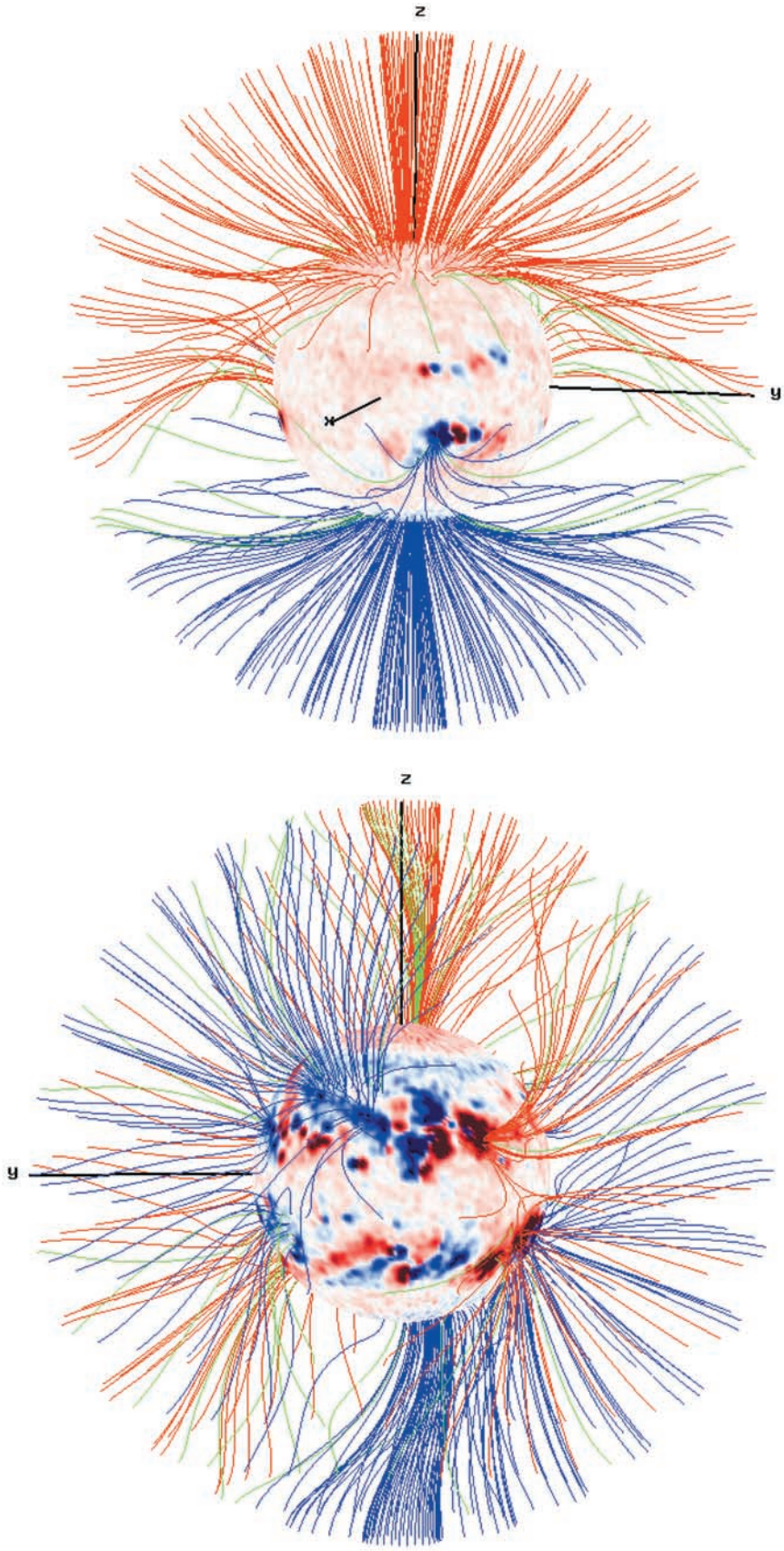

Figure 3. Open magnetic field lines between the photosphere and the source surface near (top) solar minimum and (bottom) solar maximum. Outward fields are red, inward fields are blue, and the heliospheric current sheet is green.

mapping yields an active region (AR) source; the cleanest example in CR 1953 is ACE in the longitude range 180°–240°. There are also cases of mapping to ARs just outside CHs with the same polarity (e.g., ACE from longitude 125°–150° and at longitudes >330°). We feel that for those cases the accuracy of the mapping procedure is not sufficient to state with confidence whether the source is AR or CH.

[16] At solar activity minimum, the solar wind at Ulysses and WIND mapped to the polar coronal holes, to the boundaries of those holes, or to low-latitude coronal holes [*Neugebauer et al.*, 1998]. As illustrated by Figure 2c, the sources are quite different near solar maximum when active regions are an additional source of solar wind. Furthermore, even when polar coronal holes exist, they do not appear to contribute to the wind at Ulysses at the −34° latitude of CR 1953 as shown in Figure 2c, nor at latitudes of −42° (CR 1957) or −52° (CR 1961) which are not shown.

[17] Two views of the HMF determined by the PFSS model are shown in Figure 3. These drawings trace field lines uniformly spaced every 10° in latitude and longitude on the source surface at 2.5 R_s to the photosphere. The top plot shows the calculated field configuration for CR 1893, which corresponds to the Ulysses equatorial crossing in March 1995, near solar minimum. The bottom plot is for CR 1953 near solar maximum. Once again, outward (inward) fields are shown in red (blue). The green lines correspond to the heliospheric current sheet which lies near the solar equator at solar minimum and is very highly inclined near solar maximum. A major difference between the two configurations is that at solar maximum, field lines originating at mid latitudes tend to bend up to higher latitudes. At solar minimum, on the other hand, all the high-latitude HMF originates in the polar coronal holes, and field lines originating at high and middle latitudes bend toward the equator.

4. Differences Between Coronal-Hole and Active-Region Flows

[18] In this section we address the question of whether or not there are any systematic differences between the solar wind emanating from active regions and from coronal holes near solar maximum. The detailed properties of the wind are most easily investigated when displayed as a function of time rather than source longitude. To this end we use the conversion of time at spacecraft to source surface longitude as displayed for CR 1953 in Figure 4. For ACE, there is a nearly monotonic, inverse relation between time and source longitude. Because there is nearly a 180° longitudinal separation of Ulysses and ACE, the source longitude of the Ulysses observations starts near 200°, goes through 0° to 360°, and ends up near 180° at the end of the rotation. The CR 1953 data starts at a later time at Ulysses than at ACE because Ulysses is farther from the Sun and the solar wind travel time is greater.

[19] Figure 5 shows eight different plasma parameters calculated from the Ulysses data for CR 1953. From top to bottom are (1) the proton speed V, (2) the ratio V^2/T, where T is the proton temperature, (3) the entropy per proton defined as $S = \ln(T^{3/2}/N)$, where N is the proton density, (4) the polarity of the HMF as defined in equation (1), (5) the proton $\beta_p = 8\pi NkT/B^2$ where k is the Boltzmann constant

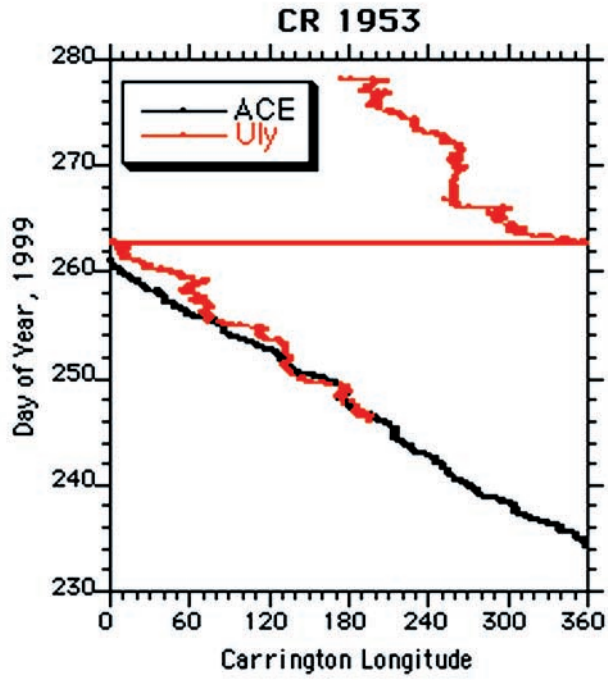

Figure 4. The connection between the time of observation of the solar wind at ACE (black) and Ulysses (red) and the mapped-back longitude on the source surface for CR 1953. Hourly averaged data are used.

and B is the magnetic field strength, (6) the ratio of alpha particle to proton densities, (7) the ratio of the densities of O^{7+} to O^{6+} ions, and (8) the average charge state of Fe ions. The first six parameters are hourly averages from the SWOOPS instrument [*Bame et al.*, 1992] and the vector helium magnetometer [*Balogh et al*, 1992]. The last two parameters are 3-hour averages of SWICS [*Gloeckler et al.*, 1992] data.

[20] The classification of source type as CH or AR was derived from Figure 2c. The source was assumed to be a coronal hole (or an active region) if the head of the arrow for a certain longitude, which corresponds to a certain time of observation at the spacecraft, landed on a coronal hole (or a region of strong field). We note that the designation of an active-region source depends only on the presence of strong fields as seen in the magnetogram; not all the AR sources correspond to numbered active regions. The classification of CH or AR is written above the trace of speed at the top of Figure 5 and vertical lines separate the wind from different sources. A few fine-scale adjustments to the positions of the lines were made on the basis of the times of HMF polarity changes. The notation WP denotes intervals in which the mapping identified a source region with the wrong magnetic polarity (i.e., red arrow to a blue source region or vice versa).

[21] The plasma and field parameters presented in Figure 5 were selected largely to assist in the identification of plasma associated with coronal mass ejections (CMEs) whose sources are not expected to be well mapped using synoptic magnetograms. Specifically, to remove CMEs from the data set we looked for the high values of V^2/T, low values of S and β_p, high values of N_α/N_p, O^{7+}/O^{6+}, and iron charge

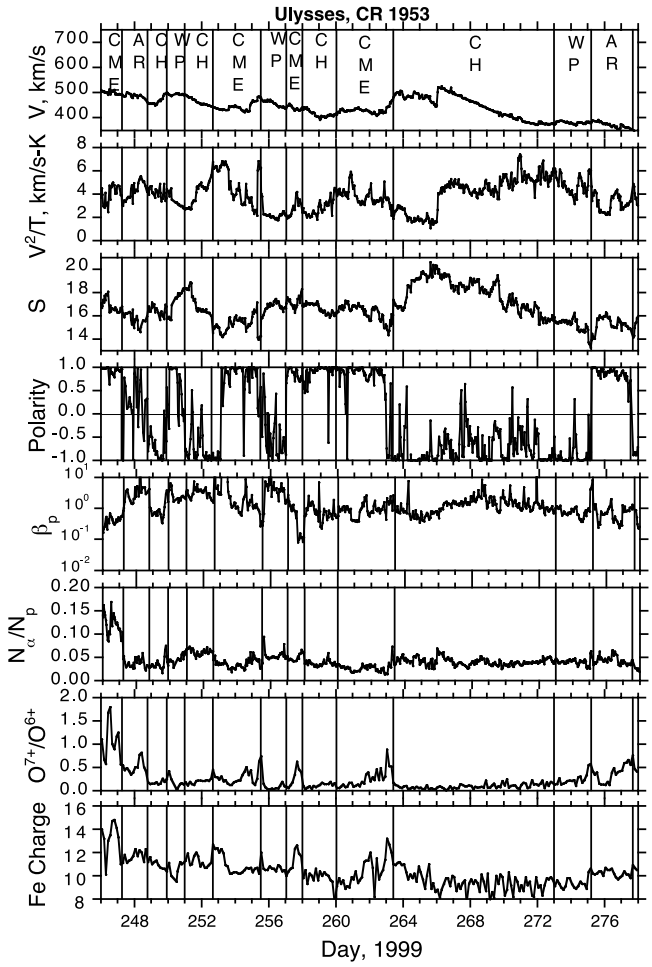

Figure 5. Time series of several plasma parameters observed by Ulysses during CR 1953. From top to bottom are solar wind speed V; the ratio V^2/T (indicative of the over-expansion frequently observed in CMEs) where T is the proton temperature; the entropy per proton, defined as $S = \ln(T^{3/2}/N)$, where N is the proton density; the polarity P of the magnetic field, as defined in equation (1); the proton $\beta_p = 8\pi NkT/B^2$, where k is the Boltzmann constant and B is the field strength; the ratio of helium to hydrogen densities; the ratio of the densities of O^{7+} to O^{6+} ions; and the average charge state of iron ions. The vertical lines denote boundaries between the solar wind that maps to different photospheric sources. The notation of source type is CME, possible coronal mass ejection; AR, active region; CH, coronal hole; and WP, wrong polarity.

state, and the presence of counterstreaming suprathermal electrons (not plotted) indicative of CMEs [*Gosling*, 1996; *Neugebauer and Goldstein*, 1997; *Galvin*, 1997; *Gosling and Forsyth*, 2001]. In questionable cases, we classified the data as CME-associated in order to minimize the CME contamination of quasistationary flows from coronal holes and active regions. Additional lines were then drawn in Figure 5 to show the limits of these possible CME events, thereby taking bites out of CH and AR intervals. The reader is warned not to use our identification of CMEs as definitive because some of our "CME" events may not in fact be transient flows.

[22] Figure 6 shows similar data for CR 1953 for ACE. The plasma data are from the SWEPAM instrument [*McComas et al.*, 1998], the field polarity from the magnetometer [*Smith et al*, 1998], and the heavy ion data from ACE/SWICS [*Gloeckler et al.*, 1998]. The notation of source type at the top of Figure 6 is the same as for Figure 5 with the addition of a type ARCH to designate mapping to an active region right next to a coronal hole with the same polarity. In such cases the accuracy of the mapping procedure may be inadequate to distinguish between the two sources. For example, the ARCH solar wind seen at ACE on days 250–252 is at longitudes of 125°–160° (see Figure 2) where the arrowhead tips are on the band of negative field just south of the coronal hole which may have been the true source of the wind.

[23] Two striking features of Figures 5 and 6 are the absence of any very fast solar wind as seen at high latitudes at solar minimum and the relatively large number of different sources. Even though the ACE magnetic polarity data in Figure 6 show a 4-sector structure, which is commonly observed during this phase of the solar cycle, there are about twice that number of different sources and peaks in the curve of speed versus time. The Ulysses profiles (Figure 5)

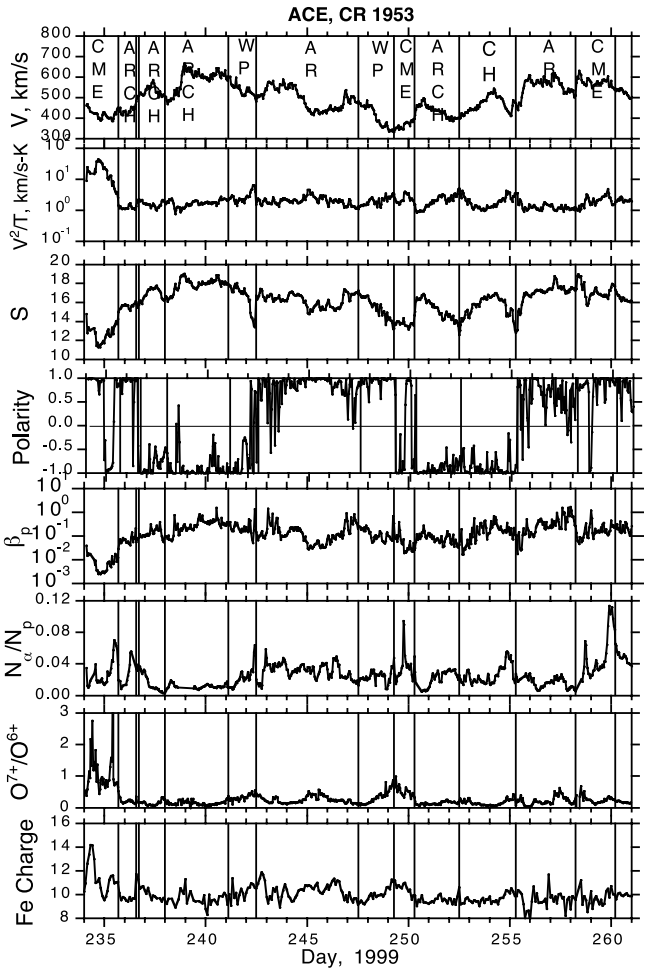

Figure 6. The same as Figure 5 except that the data were acquired by ACE. An additional source type is ARCH, an active-region source immediately adjacent to a coronal hole with the same magnetic polarity. The very short interval without a label on day 236 had the wrong polarity.

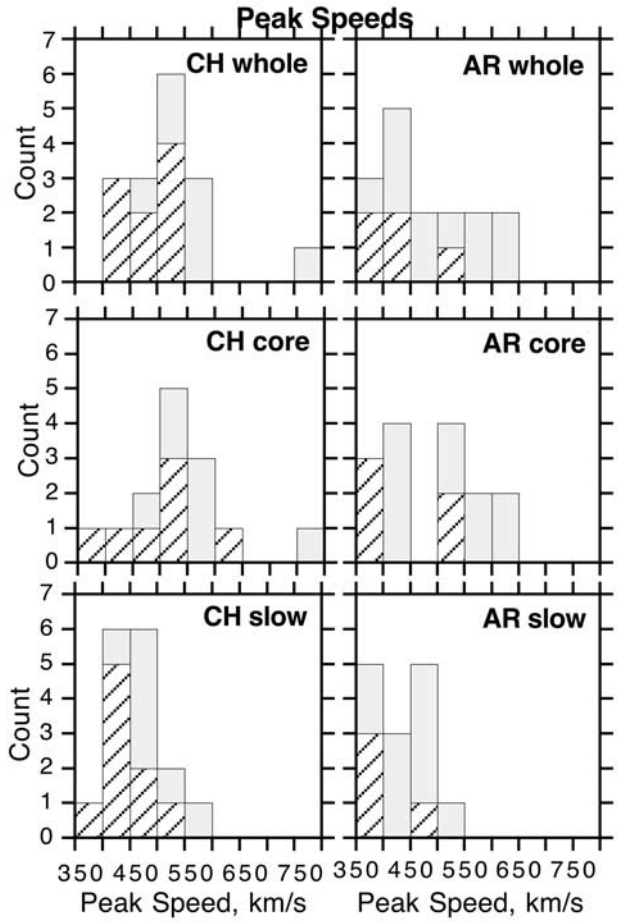

Figure 7. Histograms of the peak speeds of solar wind streams observed by ACE and Ulysses (striped) sorted according to whether the source was a coronal hole (CH) or an active region (AR). Each source (denoted by ''whole'') is subdivided according to whether it came from the Core between stream interfaces or from the Slow wind outside the stream interfaces.

are also more complex than are profiles seen at mid latitudes near solar minimum.

[24] We carried out analyses similar to the CR-1953 analysis described above for CRs 1934, 1946, and 1957. The four rotations provided 16 samples of CH flow (nine observed by Ulysses and seven observed by ACE) and 16 samples of AR flow (five observed by Ulysses and 11 observed by ACE), not including the indeterminate ARCH flows. Averages of the peak speed V, the entropy per proton S, the alpha to proton ratio N_α/N_p, and the oxygen charge state ratio O^{7+}/O^{6+} were computed for each of the 16 CH and 16 AR intervals. Histograms of the spreads of those average parameters are plotted in the top panels of Figures 7–10. The designation ''whole'' is intended to imply that the entire intervals between the vertical lines shown in the examples in Figures 5 and 6 were included in the averages. The Ulysses intervals are distinguished from the ACE intervals by diagonal hatching. With the possible exception of the O^{7+}/O^{6+} ratio, there seems to be no statistically significant difference in these four parameters between the CH-whole and the AR-whole samples.

[25] A possible reason for there being little, if any, difference between the average values of parameters in CH and AR flows is that both fast and slow wind often map back to the vicinity of the same source region. In Figure 5 see, for example, the Ulysses CH stream on days 263–272. Near the front of flows from coronal holes it is often possible to identify a surface called a stream interface. Stream interfaces on the leading edges of corotating fast streams are characterized by speed and temperature increases, density decreases, entropy increases, and changes in the helium abundance and in the heavy-ion abundances and charge states [*Burlaga*, 1974; *Gosling et al.*, 1978; *Wimmer-Schweingruber et al.*, 1997; and *Burton et al.*, 1999]. These changes are often very abrupt; about one third of them are tangential discontinuities [*Gosling et al.*, 1978]. A stream interface is more difficult to identify on the trailing edge of a high-speed stream, but *Burton et al.* [1999] were able to identify trailing-edge stream interfaces in streams from the polar coronal holes observed by Ulysses on the basis of jumps in entropy. We use these markers to break the CH and AR intervals into subintervals which we call Core and Slow, with the Core intervals being between the leading and trailing stream interfaces and the Slow subintervals before and after the Cores. Examples are given in Figures 11 and 12, both showing ACE data in CR 1953. The stream interfaces are indicated by single vertical lines and in Figure 11 there is

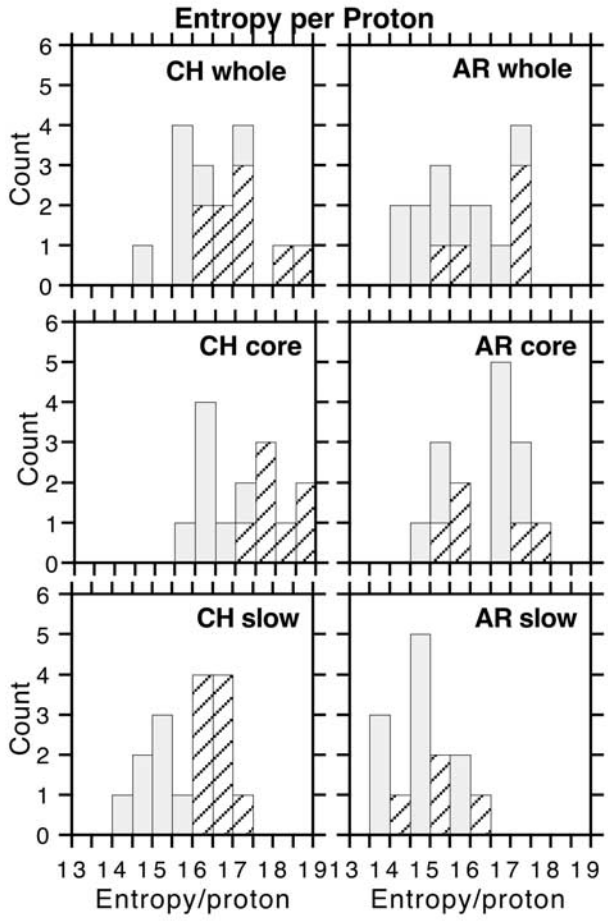

Figure 8. The same as Figure 7 except that the parameter considered is the entropy per proton.

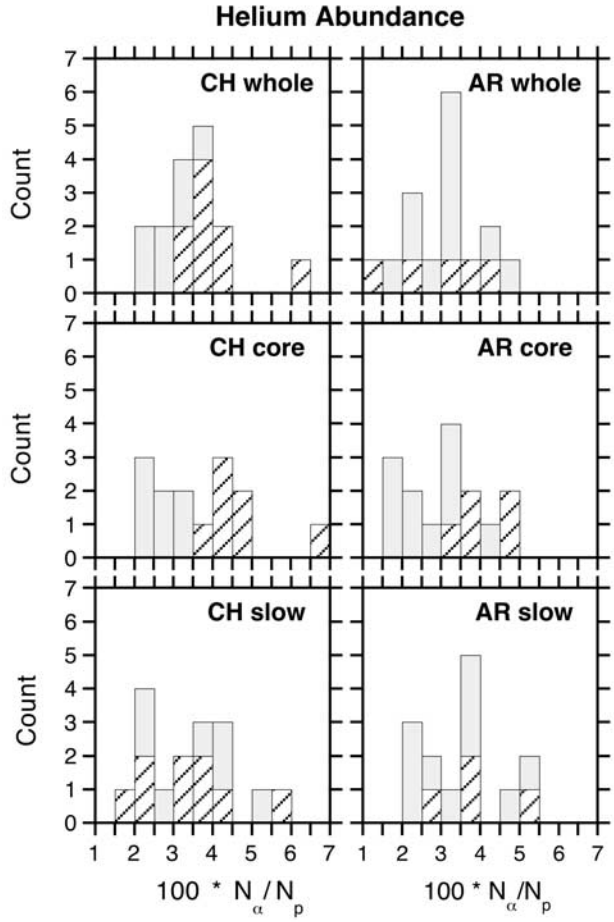

Figure 9. The same as Figure 7 except that the parameter considered is the ratio of alpha particle to proton densities.

a boundary between different source regions indicated by a double line. In some cases the exact placement of the stream interfaces is somewhat subjective and in a few other cases none can be identified. We note that the trailing-edge stream interfaces we have marked near 1530 UT on day 251 and 1900 on day 254 in Figure 11 had small, but rather abrupt changes in O^{7+}/O^{6+}; this differs from the more gradual transitions reported by *Zurbuchen et al.* [1999] for some other streams observed by ACE. In Figure 12 we have identified two Core subintervals from a single AR source. One might have broken the second AR Core subinterval in Figure 12 into two Cores with a short Slow sub-subinterval in the middle, and the first AR Core subinterval might be considered to be a series of a number of Core-Slow flows. This was typical of the wind from AR sources. Whereas the CH sources usually had only a single Core (e.g., days 253–254 in Figure 11), the AR sources often had several (e.g., Figure 12).

[26] The center and bottom panels of Figures 7–10 show histograms of separate Core and Slow subinterval averages for the CH and AR (but not ARCH) sources. There are slightly fewer Core and Slow intervals than Whole intervals because we could not always find credible stream interfaces. Table 2 provides numerical values of the average distributions; the second column is the absolute value of the difference in the average values for CH and AR sources normalized by a joint standard deviation. For these averages, the only significant difference (but only at the 1σ level) between the CH and AR histograms is that the O^{7+}/O^{6+} ratio is lower in CH than in AR flows. Although the statistics are poor, one might surmise from the two middle panels of Figure 10 that there are two populations of AR cores, one with ionization states similar to that in the cores of CH flows and the other more highly ionized. The peak speeds and the entropies are lower for the Slow wind than for the Core wind, essentially by definition. There is no statistically significant variation in N_α/N_p between one type of flow and another. Looking beyond the overall averages, however, other, more qualitative differences are apparent. In peak speed (Figure 7), AR-whole has data in the speed range 350–400 km/s, whereas CH-whole does not. In Figure 8, CH-whole and CH-core have large entropies whereas AR-whole and AR-core do not, and in Figure 9, AR-whole has data at $N_\alpha/N_p < 0.02$ whereas CH-whole does not. These trends are in accord with our preconceptions of coronal holes as generating fast, high-entropy wind with intermediate values of N_α/N_p.

5. Source Boundaries

[27] During the course of a solar rotation, there are many boundaries between different solar wind sources. Some of

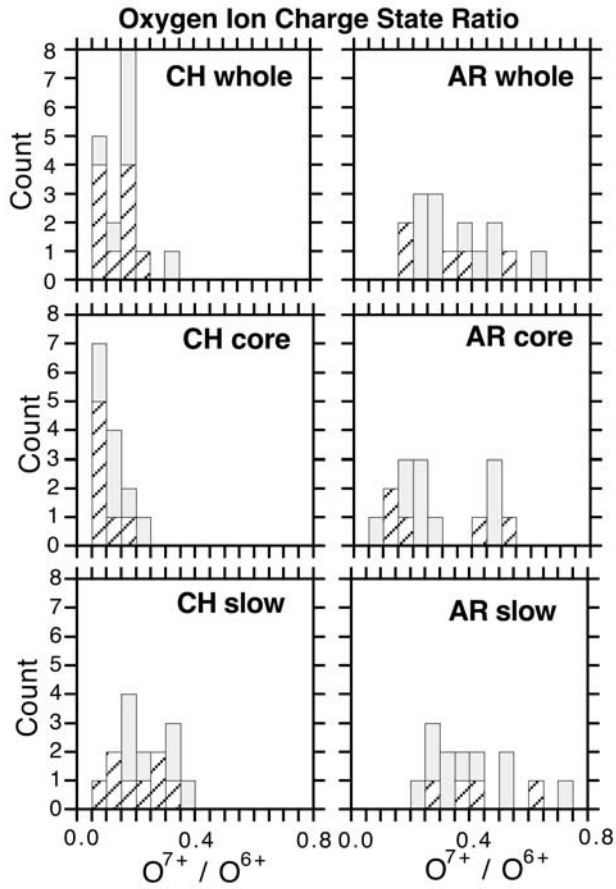

Figure 10. The same as Figure 7 except that the parameter considered is the ratio of the densities of O^{7+} to O^{6+} ions.

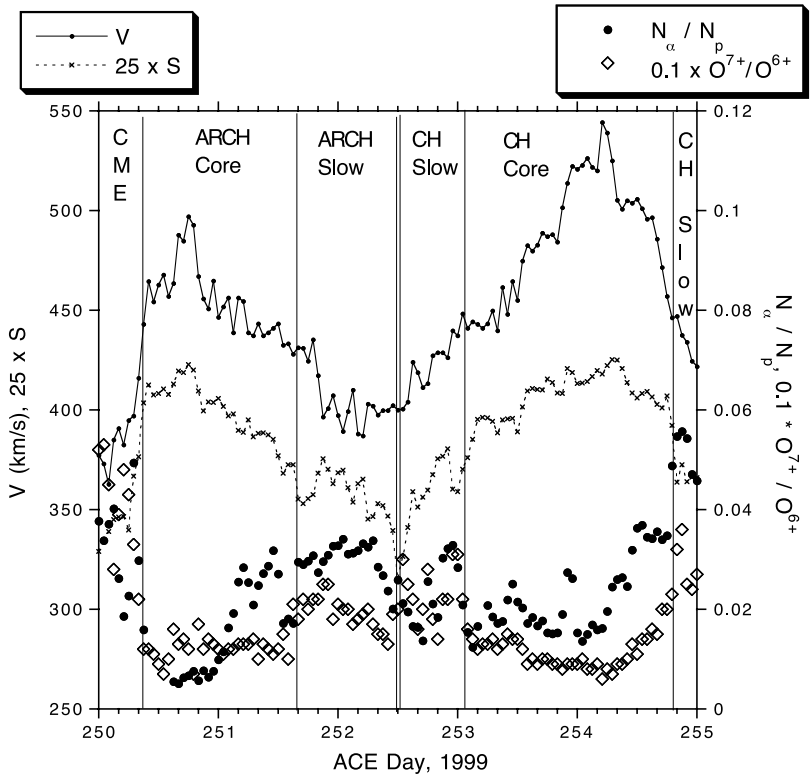

Figure 11. Higher resolution of some of the parameters plotted in Figure 6 with the addition of indications of the stream interfaces (single lines) which divide the Core and Slow parts of the flow from a single source region. The double line marks the boundary between source regions.

them are marked by a change in the polarity of the magnetic field, while others correspond to adjacent source regions with the same polarity. An example of the latter can be seen in the ACE data in Figure 2c at 128° longitude. Not only does the mapping indicate a change of source from one region of negative polarity to another, but the corresponding time series between days 250 and 255 (Figure 6) show two distinct stream structures with rising and then falling speeds.

[28] A structure called a magnetic hole is often found at or near a large-scale polarity reversal, which is variously called a magnetic sector boundary or the heliospheric current sheet [*Klein and Burlaga*, 1980]. Focusing on plasma data in addition to magnetic field data, *Winterhalter et al.* [1994] studied what is almost certainly the same phenomenon, finding a heliospheric plasma sheet (HPS) surrounding or adjacent to the HCS. The HPS is characterized by low field strength, high density, and usually low temperature. On the basis of these plasma properties, one expects to see a minimum in the entropy S near magnetic polarity changes. This dip in S at polarity reversals shows up quite clearly in the Ulysses data on days 253, 255, 263, and 275 in Figure 5 and in the ACE data on days 234, 242, 249–250, and 255 in Figure 6. What we believe has not been previously noted is a similar dip in S at interfaces between plasmas from neighboring sources with the same polarity. An example of this, corresponding to the previously mentioned source change at 128° longitude in CR 1953, can be seen in the ACE data at day 252.5 in Figures 6 and 11. The minimum in the hourly averaged value of S maps to a longitude of 124° which is within 4° of the modeled boundary between different source regions. Higher resolution data for the day 252 magnetic hole/plasma sheet are plotted in Figure 13. From top to bottom are 16-s values of the magnetic field magnitude and 64-s values of the proton density N and the entropy S. The ~4-hour duration of this magnetic hole is extremely long compared to magnetic holes that have no association with the HCS [*Turner et al.*, 1977; *Winterhalter et al.*, 1995].

[29] This example of a long-duration magnetic hole near a source boundary without a polarity change is not unique. A similar event was seen at ACE at 0900 UT on day 62, 1999. In that case, one source was a southern coronal hole at ~110° longitude (CR 1946) and the other was a northern coronal hole at ~90° longitude; both holes had negative magnetic polarity. As in the example shown in Figures 11 and 13, each source had a distinct stream structure and there was a deep entropy dip between them. We hope to investigate these source-boundary structures in greater detail in a separate paper.

6. Stream Evolution

[30] Some properties of the radial evolution of solar wind streams can be gleaned from Figures 7–10. Figure 7 shows that the peak speeds of both the CH and the AR streams tend to be lower at Ulysses between 3.6 and 5.4 AU than they are at ACE at 1 AU. This is a well known effect of stream-stream interactions. A good example is available from CR 1934 when Ulysses and ACE were at the same heliographic latitude (6°S) but at different distances from

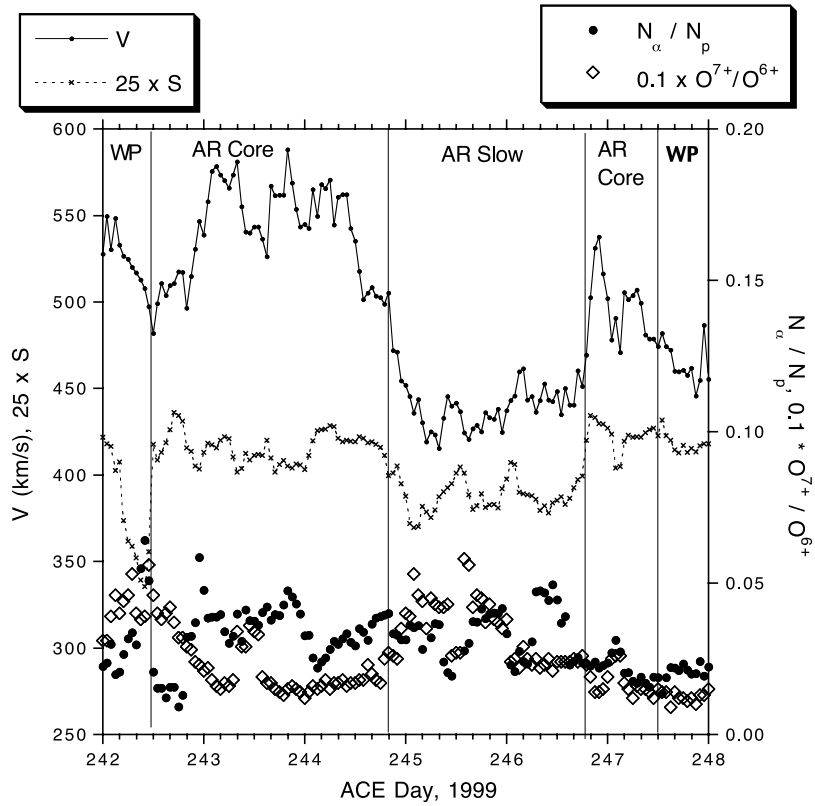

Figure 12. The same as Figure 11 for an earlier time interval when all the wind mapped to a single active region.

the Sun. Figure 14 is a plot of hourly averaged solar wind speed versus mapped-back Carrington longitude on the source surface. Ulysses data are plotted as pluses and ACE data are plotted as points. HMF polarity is coded by red or blue color. The circled data indicate hours with some signs of transient (CME) flow. For ACE, the speed versus longitude profile shows typical steep declines, called dwells, on the trailing (lower-longitude) edges of high-speed streams; dwells are especially prominent at longitudes of 170°, 230°, and 340°. While the speed at ACE ranged from 280 to 600 km/s over the course of the rotation, the speed at Ulysses remained between 350 and 460 km/s. We attribute the difference to stream-stream interactions between 1 and 5.1 AU. Despite the destruction of the velocity structure, however, the alternating sectors of positive and negative magnetic polarity are easily seen in the data from both spacecraft with only minor differences in the mapped longitudes of the sector boundaries.

[31] Figure 8 shows that the entropy per proton S was systematically greater at Ulysses than at ACE. This could also be an evolutionary effect as wave-particle interactions increase the entropy as the plasma flows away from the Sun. The difference between spacecraft is more pronounced for CH than for AR sources, perhaps because of a greater wave content of CH flows. Figure 9 suggests a higher helium abundance for CH Cores observed by Ulysses than for CH Cores observed by ACE. This difference could perhaps be attributed to differences between low-latitude and high-latitude coronal holes, but no such difference has been previously reported. Finally, in Figure 10 there is very little difference in the O^{7+}/O^{6+} ratios seen by the two spacecraft.

7. Discussion

[32] We have reached several conclusions from the analyses presented in the preceding sections. Because we focused on only a small number of solar rotations for

Table 2. Statistical Significance Between CH and AR Samples of Differences of Parameters Shown in Figures 7–10

Parameter and regime	$\frac{\lvert x_{CH}-x_{AR}\rvert}{\sqrt{\sigma_{CH}^2+\sigma_{AR}^2}}$
V_{peak}	
Whole	0.38
Core	0.41
Slow	0.46
Entropy/proton, S	
Whole	0.54
Core	0.59
Slow	0.96
N_α/N_p	
Whole	0.31
Core	0.29
Slow	0.00
O^{7+}/O^{6+}	
Whole	1.22
Core	1.08
Slow	1.18

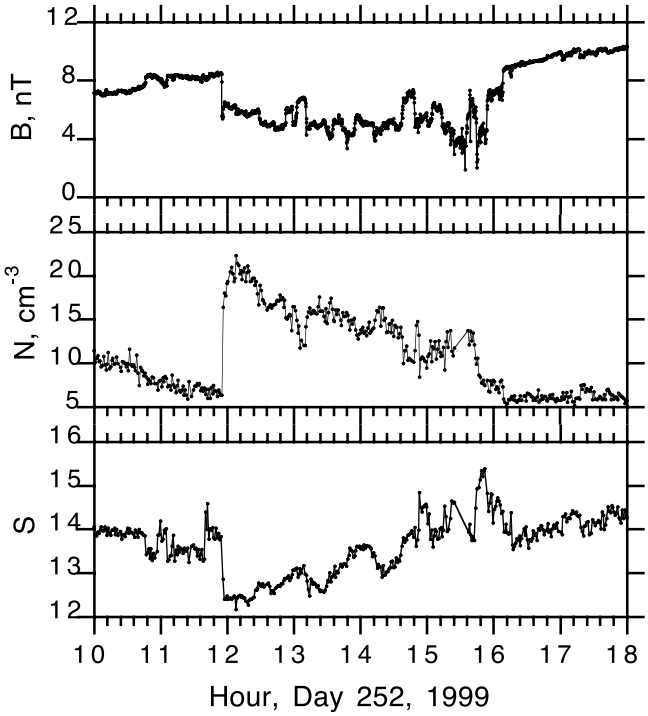

Figure 13. The highest time resolution of the magnetic field B, the proton density N, and the entropy per proton S observed by ACE at the boundary between two source regions with the same magnetic polarity.

detailed study, some of the results are more indicative than statistically inescapable. We believe, however, that our results present a consistent picture that both tests our mapping algorithm and provides some new insights into the sources of the quasistationary solar wind at a period of high solar activity.

[33] First, we believe that the 2-stage mapping procedure works well at low and midlatitudes in that the magnetic polarity of the source regions usually agrees with the magnetic polarity of the fields observed by ACE and Ulysses. Poleward of a latitude of ~60°S, however, the model predicts purely outward magnetic fields, whereas Ulysses observed a mixture of inward and outward fields. We suggest that the problem lies largely with the difficulty of observing polar fields from the viewpoint of Earth.

[34] None of the solar wind observed by either Ulysses or ACE mapped to the small polar coronal holes present during the four solar rotations studied in detail. During this phase of the solar cycle, field lines originating at mid latitudes are seen at very high latitudes in the heliosphere, whereas at solar minimum, field lines from the polar coronal holes reach down to latitudes as low as ~20° [e.g., *Smith et al.*, 1978]. This direct magnetic connection at solar maximum between the high-latitude heliosphere and midlatitude active regions should be observable in the propagation of solar energetic particles from the Sun to Ulysses.

[35] Near solar maximum, the properties of the solar wind that traces back to coronal holes are very different from the properties of the wind from polar coronal holes observed at solar minimum. The peak speed is much lower; compare Figure 7 to the 750–800 km/s flow from the polar coronal holes near solar minimum [*Phillips et al.*, 1995]. The peak speeds in our sample are closer to those observed from the mid- and low-latitude coronal holes during the Ulysses fast latitude scan in 1995 [*Neugebauer et al.*, 1998]. Such a difference in peak speeds between solar minimum and solar maximum had been predicted by *Wang and Sheeley* [1997] on the basis of their expansion-factor model. The oxygen ionization state is also different; compare Figure 10 to the O^{7+}/O^{6+} ratio of <0.03 in polar coronal holes [*von Steiger et al.*, 2000].

[36] Another major difference between this study of solar wind sources and the earlier study carried out near solar minimum [*Neugebauer et al.*, 1998] is that at times of high solar activity not only coronal holes and their boundary regions, but also active regions contribute to the quasistationary (non-CME) solar wind. The present study shows active regions producing both slow and moderately fast solar wind. Although in some cases our mapping led to sources in active regions adjacent to coronal holes where the accuracy of the mapping procedure is perhaps inadequate to determine the true source, in other cases the mapping led to active regions far from any coronal hole with the polarity of the active region agreeing with the polarity of the HMF.

[37] That active regions might be sources of solar wind is perhaps not surprising. *Levine*'s [1977] potential field models for the Skylab era (1973–1974, a period of declin-

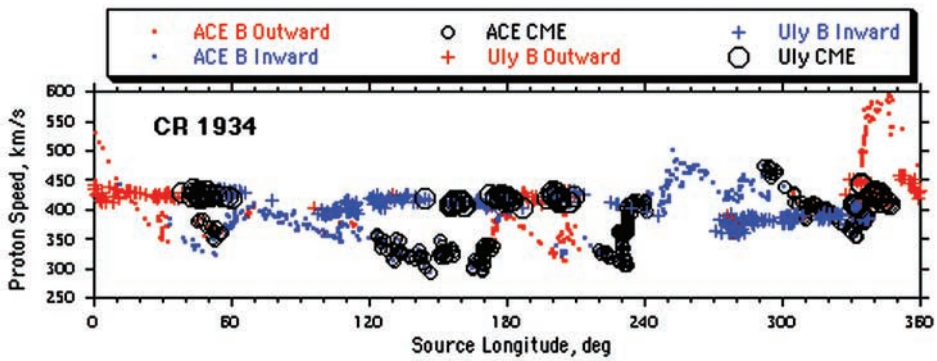

Figure 14. Solar wind speeds observed at Ulysses (pluses) and ACE (dots) as a function of longitude on the source surface during CR 1934. Intervals of outward and inward magnetic polarities are denoted by red and blue, respectively. Encircled data indicate the possible presence of a CME.

ing solar activity) showed that open field lines originate in both coronal holes and active regions. In his review article, *Levine* [1977, p. 121] states that open fields in active regions "usually lie between closed active region loops systems, along a line of separation, and are usually identifiable as small, dark X-ray features that contrast with the bright active region loop systems." On the basis of interplanetary scintillation data, *Kojima et al.* [1999] concluded that even during solar-activity minimum the slowest solar wind comes from single-polarity elements of active-region complexes rather than from the bipolar cusp regions of helmet streamers. By comparing SOHO extreme-ultraviolet observations of the Sun with the speeds and the O^{7+}/O^{6+} ratios measured in situ by SOHO, *Hefti et al.* [2000] concluded that active regions were the source of solar wind streams with moderately low speeds ($V_{peak} \approx 460$ km/s). *Liewer et al.* [2001] combined coronal data obtained by SOHO/LASCO with a PFSS model to deduce that many bright coronal streamers are caused by outflow from active regions. Perhaps even more telling because it is independent of any mapping or magnetic model are *Uchida et al.*'s [1992] Yohkoh soft X-ray observations that the corona above active regions expands outward almost continuously.

[38] Further confirmation of the reality of active regions as solar wind sources is that, even for similar speeds, the properties of CH wind are not identical to the properties of AR wind. First, there is a difference in the ratio of O^{7+}/O^{6+}. Another difference is that active-region flows often have several high-entropy cores whereas coronal hole flows have only one. It has been the recent fashion to talk of only two types of quasistationary solar wind: fast wind from coronal holes and slow wind from boundary regions. We now believe there is not such a simple dichotomy, but that in addition to slow flow from boundary regions, there are two types of faster flow from two types (CH and AR) of open field regions. The multiple cores of AR flows probably indicate either that an active region has more than one area of open field lines or that the arrangement of open and closed field lines changes in time. The difference in the O^{7+}/O^{6+} ratios may arise from different heights in the corona where the ionization is frozen in, which in turn may arise from different magnetic geometries or expansion factors. We suggest there is perhaps a hierarchy of open field regions, with the large, polar coronal holes with very fast wind and very low ionization temperatures at one extreme, smaller, low-latitude coronal holes in the middle, and open, coronal-hole-like regions in a single polarity side of active regions at the other extreme.

[39] We have introduced the term source boundary, which is distinct from the surface known as a stream interface. A magnetic sector boundary is a source boundary, but not all source boundaries are sector boundaries. All the solar wind between neighboring source boundaries maps to the vicinity of the same feature on the Sun, be it a coronal hole or an active region. For coronal hole sources, stream interfaces mark the surfaces separating the generally slow solar wind (thought by some to be produced by opening of closed field loops via reconnection with open field lines at the boundaries of coronal holes) from the flow accelerated on the continuously open field lines within the coronal hole [*Fisk et al.*, 1999; *Schwadron et al.*, 1999]. We suggest a similar scenario for active-region sources, with perhaps a collection of several regions of long-term open fields interspersed with regions of closed and reconnecting loops. Stream interfaces are marked by jumps in entropy as one goes from slow to fast wind, whereas source boundaries are marked by plasma sheets or magnetic holes and local minima in entropy.

[40] These heliospheric plasma sheets without heliospheric current sheets at the boundaries between sources with the same magnetic polarity are another discovery resulting from our analysis. These plasma sheets, or magnetic holes, have much greater thickness than most magnetic holes observed in the solar wind. In their discussion of two long-duration magnetic holes observed by three spacecraft upstream of the Earth's bow shock, *Chisham et al.* [2000] were able to rule out association with the HCS and suggested a possible conglomeration of a number of smaller holes; the present study suggests that same-polarity source boundaries may have been responsible for those large holes. *Zurbuchen et al.* [2001] studied 12 large-scale (duration 0.5 to 5 hours) magnetic holes observed by ACE in 1998, none of which corresponds to the source boundaries included in the present study. They concluded that their long-duration magnetic holes probably have a different origin than the kinetic-scale magnetic holes that may result from plasma instabilities. Instead they suggest that large-scale magnetic holes may be formed by magnetic reconnection in the high corona, between the altitude at which the ion charge states become frozen in and the sonic critical point. Although reconnection may not play a role in the large magnetic holes at same-polarity source boundaries, such an explanation cannot be ruled out. These magnetic holes at source boundaries are interesting structures ripe for further investigation. Are the bounding discontinuities tangential discontinuities, rotational discontinuities, or slow shocks? Are they in pressure balance? What are the angular distributions of suprathermal electrons? Is the composition different inside and outside the magnetic holes? What causes them?

[41] **Acknowledgments.** The NSO/Kitt Peak magnetograph data used here were produced cooperatively by NSF/NOAO, NASA/GSFC, and NOAA/SEL. We thank Jack Harvey for his assistance in using those data. The maps of coronal holes as inferred from 1083 nm He I observations made at Kitt Peak were prepared by Karen Harvey and Frank Recely as part of an NSF grant. We thank Zoran Mikic for supplying the potential magnetic field solver and field line trace programs used in this work. Jack Gosling provided input on bidirectional streaming of suprathermal electrons observed by Ulysses. The ACE magnetometer data were provided by N. F. Ness and C. W. Smith through the ACE Science Center. We thank Todd Hoeksema, Nick Arge, Jack Gosling, and Chuck Smith for helpful comments. We also thank Kristin Commer Simunac for a summer's work on the early stages of this project. Much of this work is the result of research performed at the Jet Propulsion Laboratory of the California Institute of Technology under a contract with the National Aeronautics and Space Administration. The effort at the University of Michigan was also supported by NASA. The work at Los Alamos was performed under the auspices of the U. S. Department of Energy with financial support from the NASA ACE program.

[42] Janet G. Luhmann thanks Masayoshi Kojima and another referee for their assistance in evaluating this paper.

References

Balogh, A., T. J. Beek, R. J. Forsyth, P. C. Hedgecock, R. J. Marquedant, E. J. Smith, D. J. Southwood, and B. T. Tsurutani, The magnetic field investigation on the Ulysses mission: Instrumentation and preliminary scientific results, *Astron. Astrophys. Suppl. Ser.*, *92*, 221, 1992.

Bame, S. J., D. J. McComas, B. L. Barraclough, J. L. Phillips, K. J. Sofaly, J. C. Chavez, B. E. Goldstein, and R. K. Sakurai, The Ulysses solar wind plasma experiment, *Astron. Astrophys. Suppl. Ser.*, *92*, 237, 1992.

Burlaga, L. F., Interplanetary stream interfaces, *J. Geophys. Res.*, *79*, 3717, 1974.

Burton, M. E., M. Neugebauer, N. U. Crooker, R. von Steiger, and E. J. Smith, Identification of trailing edge solar wind stream interfaces: A comparison of Ulysses plasma and composition measurements, *J. Geophys. Res.*, *104*, 9925, 1999.

Chisham, G., S. J. Schwartz, D. Burgess, S. D. Bale, M. W. Dunlop, and C. T. Russell, Multisatellite observations of large magnetic depressions in the solar wind, *J. Geophys. Res.*, *105*, 2325, 2000.

Fisk, L. A., T. H. Zurbuchen, and N. A. Schwadron, On the coronal magnetic field: Consequences of large-scale motions, *Astrophys. J.*, *521*, 868, 1999.

Galvin, A. B., Minor ion composition in CME-related solar wind, in *Coronal Mass Ejections, Geophys. Monogr. Ser.*, vol. 99, edited by N. Crooker, J. A. Joselyn, and J. Feynman, pp. 253–260, AGU, Washington, D.C., 1997.

Gloeckler, G. L., et al., The solar wind ion composition spectrometer, *Astron. Astrophys. Suppl. Ser.*, *92*, 267, 1992.

Gloeckler, G., et al., Investigation of solar and interstellar matter using solar wind and pickup ion measurements with SWICS and SWIMS on the ACE spacecraft, *Space Sci. Rev.*, *86*, 497, 1998.

Gosling, J. T., Corotating and transient solar wind flows in three dimensions, *Ann. Rev. Astron. Astrophys.*, *34*, 35, 1996.

Gosling, J. T., and R. J. Forsyth, CME-driven solar wind disturbances at high heliographic latitudes, *Space Sci. Rev.*, *97*, 87, 2001.

Gosling, J. T., J. R. Asbridge, S. J. Bame, and W. C. Feldman, Solar wind stream interfaces, *J. Geophys. Res.*, *83*, 1401, 1978.

Hefti, S., H. Grünwaldt, P. Bochsler, and M. R. Aellig, Oxygen freeze-in temperatures measured with SOHO/CELIAS/CTOF, *J. Geophys. Res.*, *105*, 10,527, 2000.

Hoeksema, J. T., Extending the Sun's magnetic field through the three-dimensional heliosphere, *Adv. Space Res.*, *9*, 141, 1989.

Klein, L., and L. F. Burlaga, Interplanetary sector boundaries 1971–1973, *J. Geophys. Res.*, *85*, 2269, 1980.

Kojima, M., K. Fujiki, T. Ohmi, M. Tokamaru, A. Yokobe, and K. Hakamada, Low-speed solar wind from the vicinity of solar active regions, *J. Geophys. Res.*, *104*, 16,993, 1999.

Levine, R. H., Large scale solar magnetic fields and coronal holes, in *Coronal Holes and High Speed Wind Streams*, edited by J. B. Zirker, pp. 103–143, Colo. Assoc. Univ. Press, Boulder, 1977.

Liewer, P. C., J. R. Hall, E. De Jong, D. G. Socker, R. A. Howard, P. C. Crane, P. Reiser, N. Rich, and A. Vourlidas, Determination of three-dimensional structure of coronal streamers and relationship to the solar magnetic field, *J. Geophys. Res.*, *106*, 15,903, 2001.

McComas, D. J., et al., Solar wind electron proton alpha monitor (SWEPAM) for the Advanced Composition Explorer, *Space Sci. Rev.*, *86*, 563, 1998.

Neugebauer, M., and R. Goldstein, Particle and field signatures of coronal mass ejections in the solar wind, in *Coronal Mass Ejections, Geophys. Monogr. Ser.*, vol. 99, edited by N. Crooker, J. Joselyn, and J. Feynman, pp. 245–251, AGU, Washington, D.C., 1997.

Neugebauer, M., et al., Spatial structure of the solar wind and comparisons with solar data and models, *J. Geophys. Res.*, *103*, 14,587, 1998.

Nolte, J. T., and E. C. Roelof, Large-scale structure of the interplanetary medium, I, High coronal source longitude of the quiet-time solar wind, *Solar Phys.*, *33*, 241, 1973.

Phillips, J. L., S. J. Bame, W. C. Feldman, B. E. Goldstein, J. T. Gosling, C. M. Hammond, D. J. McComas, M. Neugebauer, E. E. Scime, and S. T. Suess, Ulysses solar wind plasma observations at high southerly latitudes, *Science*, *268*, 1030, 1995.

Pizzo, V. J., On the application of numerical models to the inverse mapping of solar wind flow structures, *J. Geophys. Res.*, *86*, 6685, 1981.

Posner, A., T. H. Zurbuchen, N. A. Schwadron, L. A. Fisk, G. Gloeckler, J. A. Linker, Z. Mikic, and P. Riley, Nature of the boundary between open and closed magnetic field line regions at the Sun revealed by composition data and numerical models, *J. Geophys. Res.*, *106*, 15,869, 2001.

Riley, P., J. T. Gosling, D. J. McComas, V. J. Pizzo, J. G. Luhmann, D. Biesecker, R. J. Forsyth, J. T. Hoeksema, A. Lecinski, and B. J. Thompson, Relationship between Ulysses plasma observations and solar observations during the Whole Sun Month campaign, *J. Geophys. Res.*, *104*, 9871, 1999.

Schatten, K., J. W. Wilcox, and N. F. Ness, A model of the interplanetary and coronal magnetic fields, *Solar Phys.*, *6*, 442, 1969.

Schwadron, N. A., L. A. Fisk, and T. H. Zurbuchen, Elemental fractionation in the slow solar wind, *Astrophys. J.*, *521*, 859, 1999.

Smith, C. W., et al., The ACE magnetic fields experiment, *Space Sci. Rev.*, *86*, 613, 1998.

Smith, E. J., B. T. Tsurutani, and R. L. Rosenberg, Observations of the interplanetary sector structure up to heliographic latitudes of 16 degrees Pioneer 11, *J. Geophys. Res.*, *83*, 717, 1978.

Snodgrass, H. B., Magnetic rotation of the solar photosphere, *Astrophys. J.*, *270*, 288, 1983.

Turner, J. M., L. F. Burlaga, N. F. Ness, and J. F. Lemaire, Magnetic holes in the solar wind, *J. Geophys. Res.*, *82*, 1921, 1977.

Uchida, U., A. McAllister, K. T. Strong, Y. Ogawara, T. Shimizu, R. Matsumoto, and H. S. Hudson, Continual expansion of the active-region corona observed by the Yohkoh soft X-ray telescope, *Publ. Astron. Soc. Jpn.*, *44*, L155, 1992.

von Steiger, R., N. A. Schwadron, L. A. Fisk, J. Geiss, G. Gloeckler, S. Hefti, B. Wilken, R. F. Wimmer-Schweingruber, and T. H. Zurbuchen, Composition of quasistationary solar wind flows from Ulysses/Solar Wind Ion Composition Spectrometer, *J. Geophys. Res.*, *105*, 27,217, 2000.

Wang, Y.-M., and N. R. Sheeley Jr., On potential field models of the solar corona, *Astrophys. J.*, *392*, 310, 1992.

Wang, Y.-M., and N. R. Sheeley, The high-latitude solar wind near sunspot maximum, *Geophys. Res. Lett.*, *24*, 3141, 1997.

Wimmer-Schweingruber, R. F., R. von Steiger, and R. Paerli, Solar wind stream interfaces in corotating interaction regions, *J. Geophys. Res.*, *102*, 17,407, 1997.

Winterhalter, D., E. J. Smith, M. E. Burton, and N. Murphy, The heliospheric plasma sheet, *J. Geophys. Res.*, *99*, 6667, 1994.

Winterhalter, D., M. Neugebauer, B. E. Goldstein, E. J. Smith, B. T. Tsurutani, S. J. Bame, and A. Balogh, Magnetic holes in the solar wind and their relation to mirror-mode structures, *Space Sci. Rev.*, *72*, 201, 1995.

Zurbuchen, T. H., S. Hefti, L. A. Fisk, G. Gloeckler, and R. von Steiger, The transition between fast and slow solar wind from composition data, *Space Sci. Rev.*, *87*, 353, 1999.

Zurbuchen, T. H., S. Hefti, L. A. Fisk, G. Gloeckler, N. A. Schwadron, C. W. Smith, N. F. Ness, R. M. Skoug, D. J. McComas, and L. F. Burlaga, On the origin of microscale magnetic holes in the solar wind, *J. Geophys. Res.*, *106*, 16,001, 2001.

P. C. Liewer and E. J. Smith, Jet Propulsion Laboratory, California Institute of Technology, MS 169-506, Pasadena, CA 91109, USA. (paulett.c.liewer@jpl.nasa.gov; esmith@jplsp.jpl.nasa.gov)

M. Neugebauer, Lunar and Planetary Laboratory, University of Arizona, Tucson, AZ 85721, USA. (mneugeb@lpl.arizona.edu)

R. M. Skoug, Los Alamos National Laboratory, MS D466, Los Alamos, N. M. 87545, USA. (rskoug@lanl.gov)

T. H. Zurbuchen, Space Physics Research Laboratory, University of Michigan, 2455 Hayward Street, Ann Arbor, MI 48109-2143, USA. (thomasz@umich.edu)